Diagnostic Imaging of Metastatic Nodal Disease

6

Hiroko Tanaka

Abstract

Knowledge of anatomy, classification, drainage pathways, and morphologic variations of neck lymph node is key to correct interpretation of head and neck imaging. Computed tomography, magnetic resonance imaging, ultrasonography, and PET/CT are complementary imaging modalities that can be used in the evaluation of lymph node metastasis. This chapter discusses the imaging evaluation for metastatic lymph nodes in head and neck squamous cell carcinoma.

Keywords

Head and neck cancer · Neck nodal metastasis · CT · MRI · US · PET/CT

6.1 Introduction

Head and neck squamous cell carcinoma (HNSCC) comprises most common head and neck malignancy. HNSCC generally metastasizes to the cervical lymph nodes, with a frequency of approximately 50%, but the frequency varies depending on the site and stage of the primary tumor. Cervical lymph node metastasis is an important prognostic indicator in HNSCC as it reduces patient survival by 30–50%. Multiple nodes, large size, lower level metastases, and extranodal extension are additional prognostic factors. However, the smoking status and the condition of the primary tumor such as virus (human papilloma virus or Epstein-Barr virus) affect the prognosis. These characteristics and the status of the lymph node metastases influence the treatment options for surgery and/or (chemo)radiotherapy. Therefore, accurate detection of metastasis is essential, and imaging plays an integral role in every stage from initial diagnosis to posttreatment surveillance.

In this chapter, we will review the normal nodal anatomy, classification, and lymphatic drainage in the head and neck region and also will discuss imaging techniques, the imaging criteria, treatment assessment, and post-therapeutic surveillance for metastatic lymph nodes of HNSCC patients.

6.2 Anatomy of Normal Lymph Node

In the head and neck region, there are 150–350 lymph nodes equivalent to one third of the whole body lymph nodes. The lymph nodes are flat lumpy peripheral lymphoid organs.

The afferent lymphatic vessels are on the capsule side of the lymph nodes, and the efferent lymphatic vessels pass through the hilum. The blood supply of the lymph nodes is through the arteries entering from the hilum. The venous blood of the lymph node is collected in the medulla and leaves the lymphatic hilum.

Lymph code is divided into cortex, paracortex, and medulla from the outside. The cortex has numerous lymphoid follicles as B lymphocyte areas. Lymphoid follicles are primary follicles that do not undergo antigen stimulation and secondary follicles that have germinal centers formed by differentiation and proliferation of B lymphocytes under antigen stimulation. The secondary follicle is composed of the germinal center and the mantle zone in which the primary follicle surrounds the germinal center. The paracortex is mostly occupied by T lymphocytes. The medulla exists from the deep paracortex to the hilum, and the small lymphocytes and many plasma cells are distributed in the medulla, resulting in humoral immunity.

The lymph sinus is a lymphatic flow pathway. There are small lymphocytes and sinus histiocytes in the sinus. Lymph fluids draining from the lymphatic vessels that penetrate the lymph node capsule pass through the marginal sinuses, the intermediate sinuses, and the medullary sinuses and are poured from the lymph nodes into the efferent lymphatics.

H. Tanaka (✉)
Department of Diagnostic Imaging, Cancer Institute Hospital, Japanese Foundation for Cancer Research, Koto-ku, Tokyo, Japan
e-mail: hiroko.tanaka@jfcr.or.jp

H. Ojiri (ed.), *Diagnostic Imaging in Head and Neck Cancer*, https://doi.org/10.1007/978-981-15-3188-0_6

The lymph node acts as a filter and plays a role in protecting the body. When antigens, cell fragments, bacteria, and cancer cells are filtered out in the lymph node, the lymphocytes and phagocytes in the lymph node react and the lymph node enlarged. Lymph node metastasis occurs when the filtered cancer cells proliferate in the lymph nodes and often begins in the marginal sinus.

6.3 Lymph Node Classification

The classification of Rouvière in 1938 has been the basis of all the current nodal classification and most commonly used [1]. In 1998, the American Head and Neck Society and American Academy of Otolaryngology-Head and Neck Surgery proposed a new nodal classification with the development of more advanced surgical approaches to head and neck cancer. This system could accurately reflect lymphatic drainage patterns; however, some of the surgical boundaries were difficult to define by imaging. The imaging-based classification by Som et al. in 1999 used well-defined anatomic boundaries that can be easily identified and highly reproducible by both clinicians and radiologists [2]. The imaging-based classification has been widely accepted and applied for initial evaluation and surveillance of HNSCC patients regardless of the method of treatment (Fig. 6.1).

It is important to note that the imaging-based level classification does not include several anatomic groups, such as supraclavicular, retropharyngeal, occipital, parotid, facial, and other superficial nodes discussed in the basic anatomic classification; these groups continue to be referred by their terminology (Fig. 6.2).

6.3.1 Imaging-Based Classification

This classification is intended for lymph nodes for neck dissection of cancer treatment. Cervical lymph nodes can be categorized by imaging-based landmarks. Figure 6.1 summarizes the imaging-based classification except level VII.

Level I is divided into IA and IB. Level IA lymph nodes are submental nodes and found between the anterior bellies of the digastric muscles below the mandible. Level IB nodes are submandibular nodes and found lateral to the anterior bellies of the digastric muscle and anterior to the posterior margin of the submandibular glands within the submandibular space.

Level II, III, and IV nodes extend along the internal jugular vein (IJV) and are deep to the sternocleidomastoid muscle (SCM) and anterior to the posterior edge of the SCM. Level II nodes are the upper portions of the internal jugular chain and spinal accessory chain, extending from the posterior belly of the digastric muscle to the bottom of the hyoid bone. Level IIA nodes are found posterior to the posterior margin of the submandibular gland, and may be anterior, or lateral to the IJV and touching to the posterior wall of the IJV. Level IIB nodes are posterior to the IJV with a fat plane between the node and the IJV. Level III nodes are middle internal jugular chain nodes, extending from below the hyoid bone to the inferior margin of the cricoid cartilage. Level IV nodes are lower internal jugular chain nodes from the inferior margin of the cricoid cartilage to the supraclavicular fossa.

Level V nodes are found in the posterior cervical space corresponding to the spinal accessory chain, lying posterior to the posterior margin of the SCM. Level V nodes are divided into VA and VB. Level VA nodes are from skull base to the inferior of the cricoid cartilage; level VB nodes are from below level VA to the supraclavicular fossa.

Level VI nodes are in the visceral space between the carotid arteries, extending from the bottom of the hyoid bone to the top of the manubrium, including the prelaryngeal, pretracheal, and paratracheal subgroups.

Level VII nodes are the superior mediastinal nodes located between the carotid arteries from the superior margin of the manubrium to the innominate vein.

The supraclavicular nodes lie at or caudal to the level of the clavicle and lateral to the carotid artery on each side of the neck, as seen on each axial scan.

The retropharyngeal nodes lie medial to the internal carotid arteries (ICA) within 2 cm of the skull base.

6.3.2 Basic Anatomic Classification

The supraclavicular nodes are along the transverse cervical artery in the supraclavicular fossa connecting the inferior aspects of internal jugular chain (IJC) and spinal accessory chain (SAC). Although these lymph nodes are not assigned a level in image-based classification, Som et al. distinguish them from levels VB, IV, and VI as indicated in the previous section. The Virchow node is specifically named pathologic node within the left supraclavicular fossa and is clinically significant. If no primary tumor is evident in the neck, this Virchow node is a signal for pulmonary or abdominal primary tumor.

The retropharyngeal nodes (RPN) include both the medial retropharyngeal space (RPS) node found in the paramedian RPS in the suprahyoid neck and the lateral RPS node (Fig. 6.2a) found lateral to the prevertebral muscles and medial to the ICA and IJV. It is important that the RPNs are often subclinical and imaging can be the first indicator of disease.

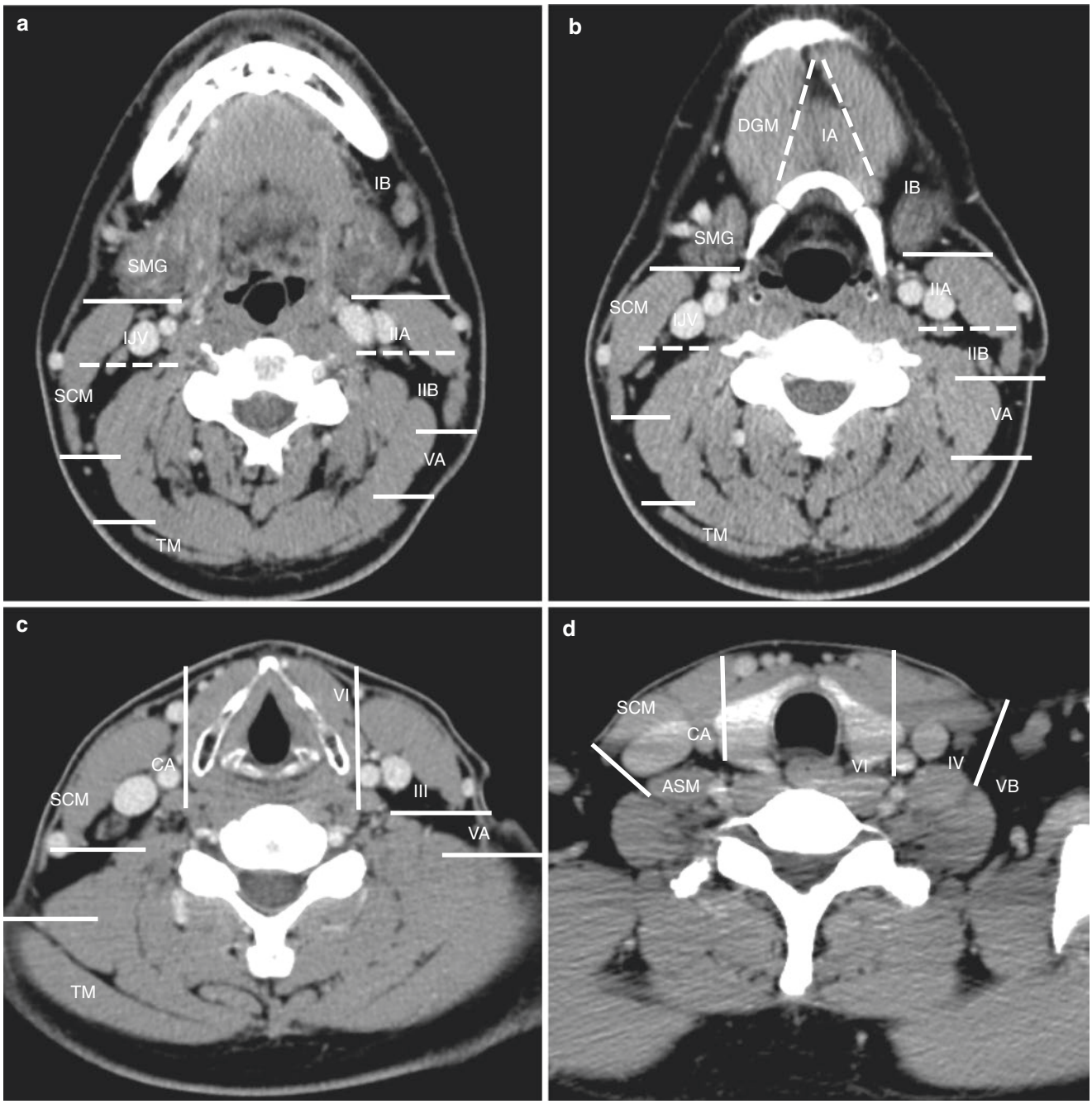

Fig. 6.1 Axial contrast-enhanced computed tomography (CECT) images show distribution of cervical node levels using the imaging-based classification. Solid lines indicate the boundaries of the nodal levels, and dotted lines indicate level subdivisions. (**a**) level IB, IIA, IIB, VA (**b**) level IA, IB, IIA, IIB, VA (**c**) level III, VA, VI (**d**) level IV, VB, VI (*ASM* anterior scalane muscle, *CA* carotid artery, *DGM* anterior belly of the digastric muscle, *IJV* internal jugular vein, *SCM* sternocleidomastoid muscle, *SMG* submandibular gland, *TM* trapezius muscle)

The occipital nodes (Fig. 6.2a) are located within the subcutaneous tissues posterior and inferior to calvarium. These nodes are divided into suprafascial/superficial, subfascial, and submuscular/subsplenius occipital nodes.

The parotid nodes (Fig. 6.2b) are located in the parotid region and are divided into three. The intraglandular nodes are within the fascia circumscribing the parotid space. The preauricular or postauricular nodes are found anterior or posterior to the auricle.

The facial lymph nodes include multiple nodes named for their anatomic location, such as the mandibular nodes superficial to the mandible (Fig. 6.2c), the buccinator nodes within

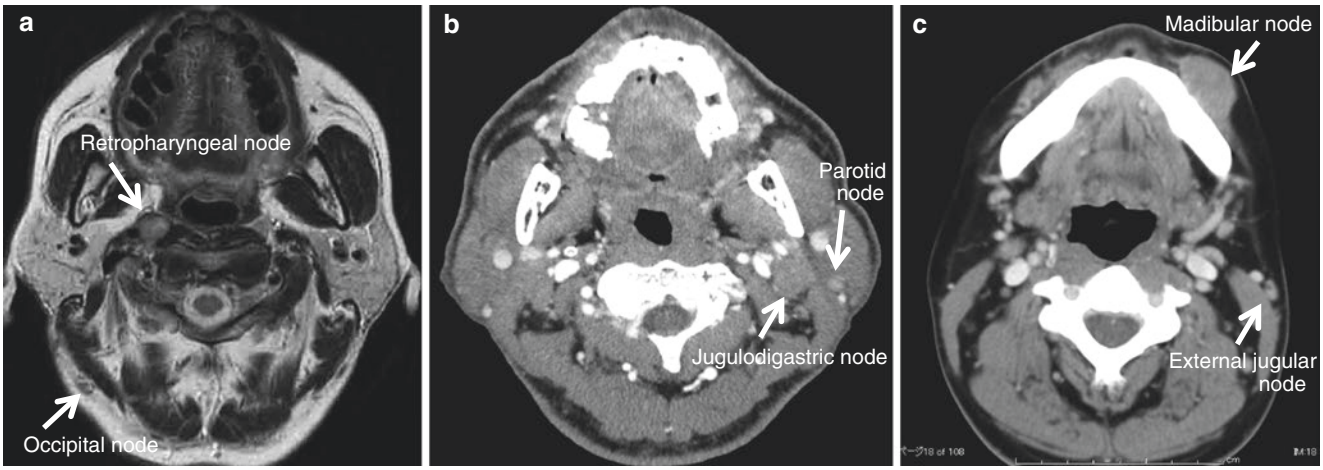

Fig. 6.2 Axial T2WI (**a**) and CECT images (**b**, **c**) show anatomic named nodes. (**a**) Retropharyngeal and occipital nodes, (**b**) jugulodigastric and parotid nodes, (**c**) madibular and external jugular nodes

the subcutaneous tissues of the cheek, the infraorbital nodes below the orbits, the malar nodes along the malar eminence, and the zygomatic nodes superficial to the zygomatic arch.

The lingual/sublingual node is along the lymphatics of the tongue. The lateral node is located in sublingual space along the lingual artery and vein. Lymph nodes between the submandibular gland and the hyoid bone, which are called parahyoid lymph nodes, are classified as lateral lingual lymph nodes. The medial node is located between both genioglossus muscles.

The external jugular node (Fig. 6.2c) is found in the superficial space along the external jugular vein.

The anterior cervical group is located in the infrahyoid anterior neck. Although the prelaryngeal, pretracheal, and paratracheal nodes are included in level VI, the anterior jugular nodes along the anterior jugular vein are not included in imaging-based classification.

The jugulodigastric node (Fig. 6.2b) is a specifically named lymph node and included in the high IJC. This node may normally be larger than other nodes and will quickly enlarge with upper respiratory infections.

6.4 Common Lymphatic Drainage of HNSCC

Lymphatic drainage patterns are important in pathologic processes. HNSCC has a common lymphatic drainage pattern of metastasis. The relationship between primary sites and lymph node metastasis of HNSCC has been well studied [3]. Knowledge of these patterns is essential when evaluating neck lymph nodes in HNSCC patients, and conversely, primary tumors can be suggested from the site of lymph node swelling. Nodal metastases of most HNSCC are present more frequently on the ipsilateral side. Contralateral metastases can also occur, and the risk increases with the presence of ipsilateral nodal metastases and increased proximity of the primary tumor site to the midline. As a general rule, when contralateral metastasis is present, it often mirrors the nodal distribution of disease in the ipsilateral neck. However, these patterns of lymphatic spread are not defined because of the many lymphatic connections, and skip metastasis to more distal nodal levels without involvement of usual proximal pathways can occur in up to 15% of cases [4]. The common lymphatic drainage pathways are discussed here.

Table 6.1 Lymphatic drainage: Main primary sites

Location	Primary site
IA	Lip, tip of tongue, anterior oral floor, skin of face
IB	Tongue, posterior oral floor, buccal mucosa, gingiva, skin of face, paranasal sinuses, submandibular gland
II	Pharynx, oral cavity, supraglottis, paranasal sinuses
III	Pharynx, supraglottis, tongue, base of tongue
IV	Larynx, thyroid, cervical esophagus, infraclavicular primary
V	Pharynx, skin of scalp, thyroid
VI	Larynx, cervical esophagus, thyroid
VII	Subglottis, cervical esophagus, thyroid
SCN	Any HNSCC, cervical esophagus, thyroid, infraclavicular primary
RPN	Nasopharynx, oral cavity, sinonasal, oropharynx, posterior wall of hypopharynx
Parotid	Orbit, nasopharynx, skin, ear, parotid

RPN retropharyngeal node, *SCN* supraclavicular node

6.4.1 Drainage Patterns to Lymph Nodes

The relationship between nodal classification of neck lymph nodes and primary sites is listed in Table 6.1.

Level I nodes receive lymphatic drainage from the lips, floor of the mouth, and oral tongue. Level IA nodes normally

drain into level IB nodes, and level IB nodes usually drain into level II.

Level II, III, and IV nodes typically receive drainage from the pharynx, oral cavity, parotid space, retropharyngeal space, facial nodes, and level I nodes. The usual pattern of lymphatic drainage progresses from level II to level III to level IV and drains into the IJV, the subclavian vein, or the transverse cervical chain.

Levels VA and VB receive drainage from the pharynx; the occipital, or mastoid, or parietal scalp region; and the lateral neck and drain into the transverse cervical chain.

Level VI receives drainage from the visceral space including the larynx, trachea, esophagus, thyroid, and dermal lymphatics of the anterior neck and typically drains into the superior mediastinum and level IV nodes.

The retropharyngeal nodes receive drainage from the sinonasal and pharyngeal mucosal surfaces and usually drain into the high level II.

The intraparotid nodes receive lymphatic drainage from the external auditory canal, the pinna of the ear, the eustachian tube, the skin of the lateral forehead and temporal region, posterior cheek, gums, and buccal mucosa and drain into the high level II.

The transverse chain receives drainage from the internal jugular chain, spinal accessory chain, subclavicular nodes, upper anterior chest wall, and skin of the anterolateral neck.

6.4.2 Drainage Patterns from the Primary Site

The lymphatic drainage pathways from each anatomic area are summarized in Table 6.2.

Table 6.2 Lymphatic drainage: Main drainage routes

Anatomic area	Subdivision	Lymphatic drainage
Nasal cavity	Anterior nose	IB
	Posterior 2/3 nose	RPN, IB, II, III
Paranasal sinus	Paranasal sinus	II, III, IB, RPN
Oral cavity	Tip of tongue	IA
	Tongue	IB, II, III
	Hard palate	II, III
	Upper gingiva	II, III
	Lower gingiva	IB, II
	Lip	IA, IB
	Buccal mucosa	IB, IIA
	Anterior oral floor	IA, II, III
	Posterior oral floor	IB, II, III
	Retromolar trigone	IB, II, III
Pharynx	Nasopharynx	RPN, II, III, IV, V
	Tonsillar fossa	II, III
	Base of tongue	II, III
	Soft palate	II, III, RPN, parotid
	Anterior tonsillar pillar	IB, II, III
	Posterior tonsillar pillar	II, III, IV, V, RPN
	Hypopharynx	II, III, IV, VB, RPN, VI
Larynx	Supraglottis	III, II, IV
	Glottis	III, II
	Subglottis	VI, IV, III
Esophagus	Cervical esophagus	VI, VII, IV, SCN
Scalp	Skin	Parotid, mastoid, occipital, V
Ear	Auricle, EAC	Parotid, mastoid, II, III
Orbit	Orbit	Preauricular, parotid, II
Salivary gland	Parotid	II, III, parotid, V
	Submandibular	IB
	Sublingual	IA, IB

EAC external auricular canal, *RPN* retropharyngeal node, *SCN* supraclavicular node

The anterior nose drains to level IB. The posterior two third nose drains to retropharyngeal nodes, levels IB, II, and III.

Drainage of the tongue is complex. The anterior tongue drains to levels IA and IB. The posterior tongue may drain to level IB or level II. Level III and IV nodes may be involved in advanced disease, or skip metastasis. Midline lesions may have bilateral pathways. Drainage of the other oral cavity may extend from level I to level IV, depending on the location of the primary tumor. Anterior regions drain to level IA nodes, and posterior portions drain preferentially to level II. Oral floor can also have relatively frequent bilateral nodal metastasis [5].

Tumors arising in the pharynx have a higher risk of presenting with nodal metastasis, and midline lesions may result in bilateral drainage patterns. The nasopharynx has rich lymphatic supply and shows one of the highest rates of nodal metastasis when involved with SCC [6]. The nasopharynx also serves as the catchment basin for lymphatic drainage of most of the nasal cavity and paranasal sinuses. The lymphatic drainage is to lateral retropharyngeal nodes and level II nodes, with drainage to more distal level III, IV, and V nodal groups in more advanced disease and through alternative drainage patterns. The drainage of oropharynx is primarily to level II and III nodal groups, with less common involvement of retropharyngeal and level IV nodes. The hypopharynx has rich lymphatic supply, particularly dense lymphatic drainage in the piriform sinuses. Drainage is similar to that of the oropharynx with predominant involvement of level II to IV and occasionally RPNs from the posterior hypopharyngeal wall. Anterior hypopharyngeal lymphatic channels may directly communicate with laryngeal lymphatics, with eventual involvement of level VI nodes.

Laryngeal drainage patterns are divided into supraglottic, glottic, and subglottic patterns. Supraglottic regions drain primarily to level III, with occasional drainage cephalad to level II. Prominent horizontal drainage patterns lead to an increased risk for bilateral metastasis. Glottic regions have poor lymphatic drainage. More advanced glottic lesions

may have involvement of nodal levels II to IV and VI. Subglottic processes have primarily lateral drainage to levels III, IV, and VI.

6.5 Imaging Techniques

The evaluation of the cervical lymph node is an essential part of the management of head and neck cancer. The nodal metastasis in HNSCC patient is a significant negative prognostic factor. Diagnostic accuracy of neck nodal metastasis is improved by the use of imaging rather than clinical palpation alone. Multiple modalities of computed tomography (CT), magnetic resonance imaging (MRI), ultrasonography (US), and fluorodeoxyglucose positron emission tomography (FDG-PET) are currently used for assessment of cervical lymph nodes (Figs. 6.3 and 6.4).

6.5.1 Contrast-Enhanced CT and MRI

CT and MRI are used for staging and surveillance of patients with HNSCC. CT is commonly used for regional nodal staging, because the short examination times reduce motion artifacts and spatial resolution is high compared with MRI [7]. Patients should be positioned with the infraorbitomeatal line, when using CT or MRI to evaluate lymph nodes.

CT is typically obtained helically from above the skull base through the tracheal carina. CT is performed using a contrast agent unless limited. Images with high-resolution CT can be reconstructed and useful for detection of lymph node metastasis.

For MR, T1-weighted images (T1WI), T2-weighted images (T2WI), diffusion-weighted images (DWI), and contrast-enhanced T1WI with fat saturation are recommended (Fig. 6.4b–e). DWI has shown promise in improving detection and characterization of lymph nodes and may be helpful in evaluating the posttreatment neck [8]. Multiple studies demonstrate that malignant nodes tend to have relative diffusion restriction with lower apparent diffusion coefficients. Some studies have shown high sensitivity (84–89%) and specificity (94–97%) for detection of metastatic nodes by DWI, exceeding conventional sequences [9, 10]. However, magnetic field inhomogeneity can reduce the image quality on DWI.

6.5.2 US

US is a convenient way to assess neck lymphadenopathy. US has better spatial resolution in evaluating internal architecture than CT or MRI (Figs. 6.3 and 6.4) [11]. US combined Doppler technique or fine-needle aspiration cytology (FNAC) is useful and improves sensitivity and specificity in diagnosis of metastatic nodes. However, interpretation is observer dependent, and retropharyngeal and mediastinal nodes cannot be assessed with US.

6.5.3 FDG-PET/CT

FDG-PET is an imaging modality that evaluates for metabolically active tissue. Integrated PET-CT units have improved the accuracy of PET image interpretation (Fig. 6.4f) [12]. FDG-PET/PET-CT is used for staging and post-therapeutic surveillance in HNSCC. Several studies have demonstrated higher sensitivity (84–92%) and specificity (95–99%) for PET/CT in the detection of regional lymph node metastases in HNSCC, compared with CT, MRI, or US [12–14]. Although PET-CT has the potential to detect small metastatic deposits in normal-sized nodes, a lower sensitivity for diagnosis of lymph nodes less than 10 mm is limitation. Other limitations are that cystic or necrotic nodes may be false negative while reactive nodes may be false positive (Fig. 6.5) [15].

6.6 Imaging Features of Metastatic Nodes

The primary method of detecting metastatic lymphadenopathy was palpation, and the criteria used were nodal size and fixation. Metastasis was suggested if a palpable node was larger than 1.5 cm in greatest diameter.

The imaging criteria were based on applying the clinical size criteria to CT and scrutinizing the features for evidence of extranodal extension in all size lymph nodes. Imaging criteria for lymph node metastasis have been reported, and the criteria shown below are widely used. However, even with these imaging criteria, occult metastases can be found in several primary lesions such as oral cavity, oropharynx, hypopharynx, and supraglottic cancers.

6.6.1 Size

Size criteria are widely used in evaluating lymph nodes. Nodes measuring greater than 15 mm in maximum diameter in level II and level IB and greater than 10 mm in all other levels are considered abnormal [16]. These criteria correspond to the earlier clinical experience described, and nodes exceeding these dimensions are metastatic by about 80%. Minimum diameter measurements are more accurate, and diameters exceeding 11 mm in level II and 10 mm elsewhere are considered abnormal (Fig. 6.4) [3]. It has been proposed that retropharyngeal nodes should not exceed 8 mm in maximum diameter or 5 mm in minimum short-axis diameter [17, 18]. On US, nodes measuring greater than 7 mm in minimum axial diameter in level II and 6 mm elsewhere are considered abnormal [19]. Although some size criteria for determination of metastatic lymphadenopathy have been proposed, unfortunately none are perfect (Fig. 6.6) [20].

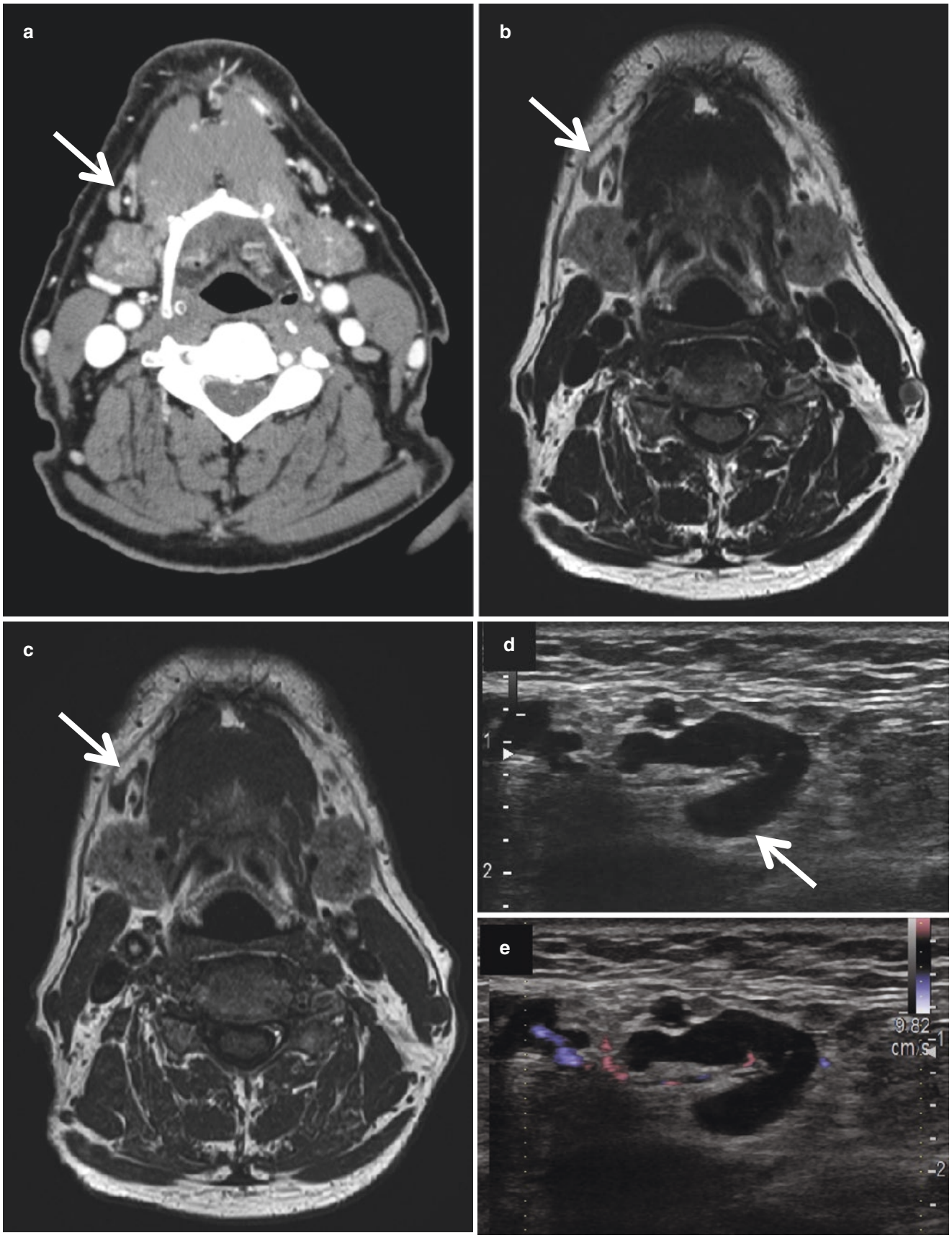

Fig. 6.3 A right level IB lymph node (*arrow*) shows normal size and shape with fatty hilum on axial CECT (**a**), T2WI (**b**), and T1WI (**c**). US shows homogeneous parenchyma (**d**, *arrow*) and echogenic hilum with a hilar vascular pattern on color Doppler (**e**)

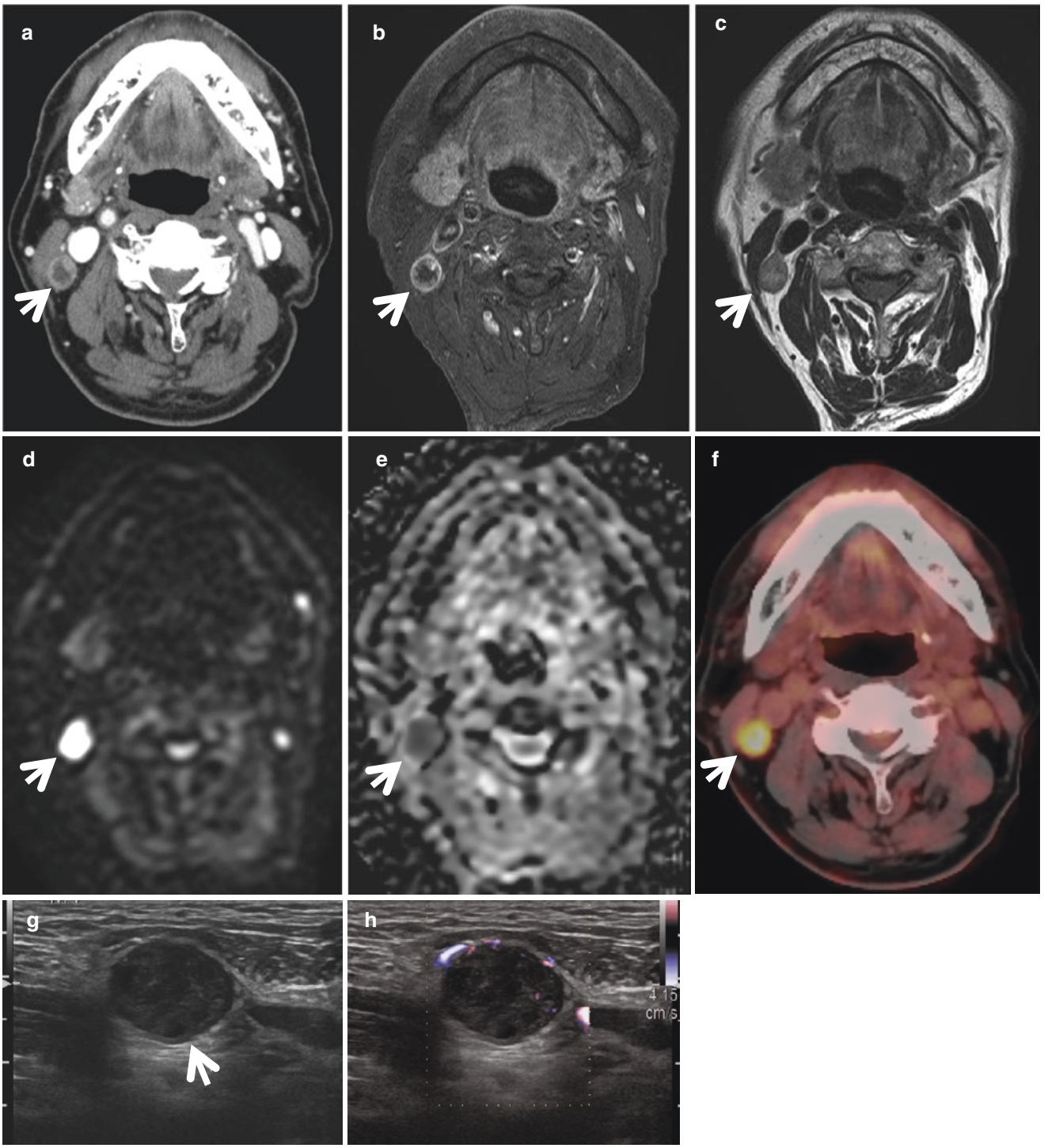

Fig. 6.4 Metastatic right level II node (*arrow*) from hypopharyngeal cancer exceeds 11 mm in minimum diameter with focal inhomogeneity on both enhanced CT (**a**) and T1WI (**b**), intermediate intensity on T2WI (**c**), restricted diffusion on DWI (**b** of 1000 s/mm^2) (**d**), a ADC of 0.74×10^{-3} mm^2/s (**e**), FDG uptake on fused PET/CT (**f**), and absent hilum and a non-hilar vascular pattern on US (**g**, **h**)

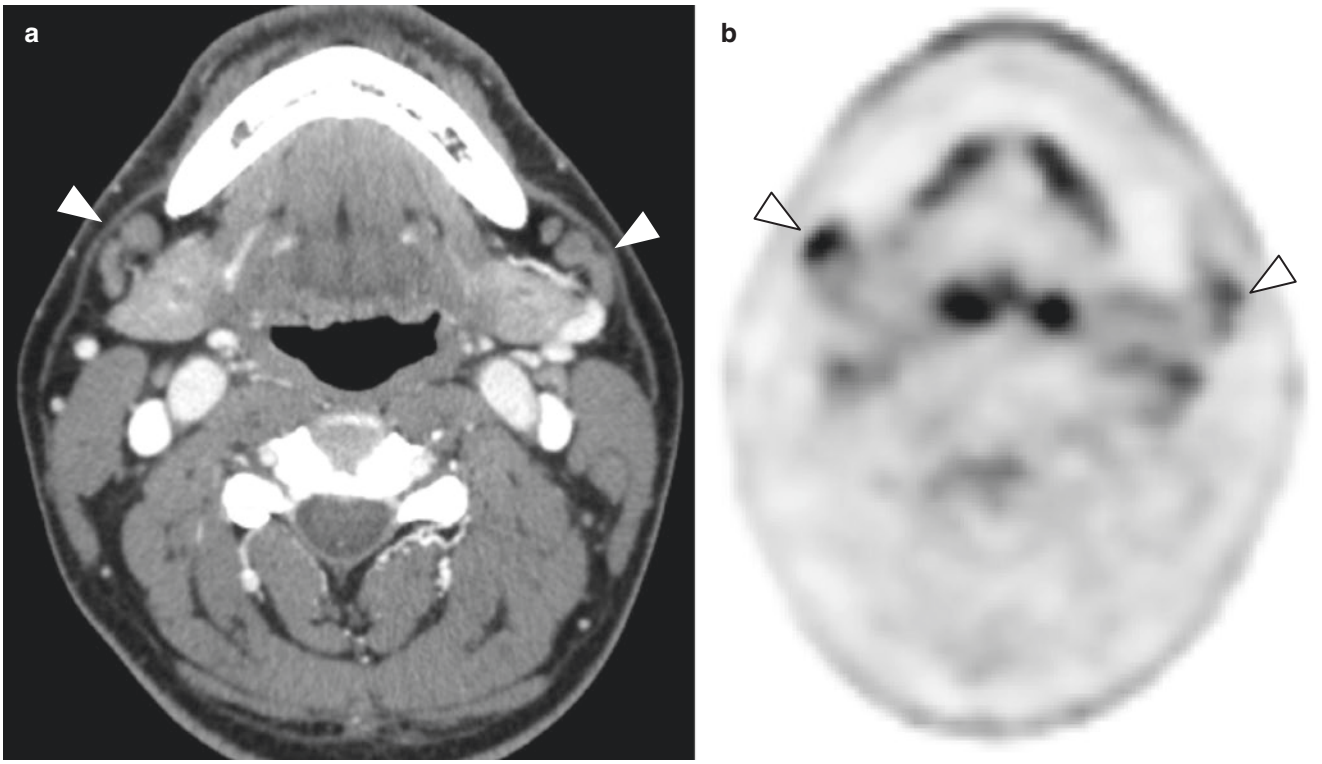

Fig. 6.5 Hyperplastic bilateral level IB nodes (**a**, **b**, *arrowhead*) reveal well-defined margin and lobulated shape on CECT (**a**). FDG-PET shows false-positive uptake (**b**)

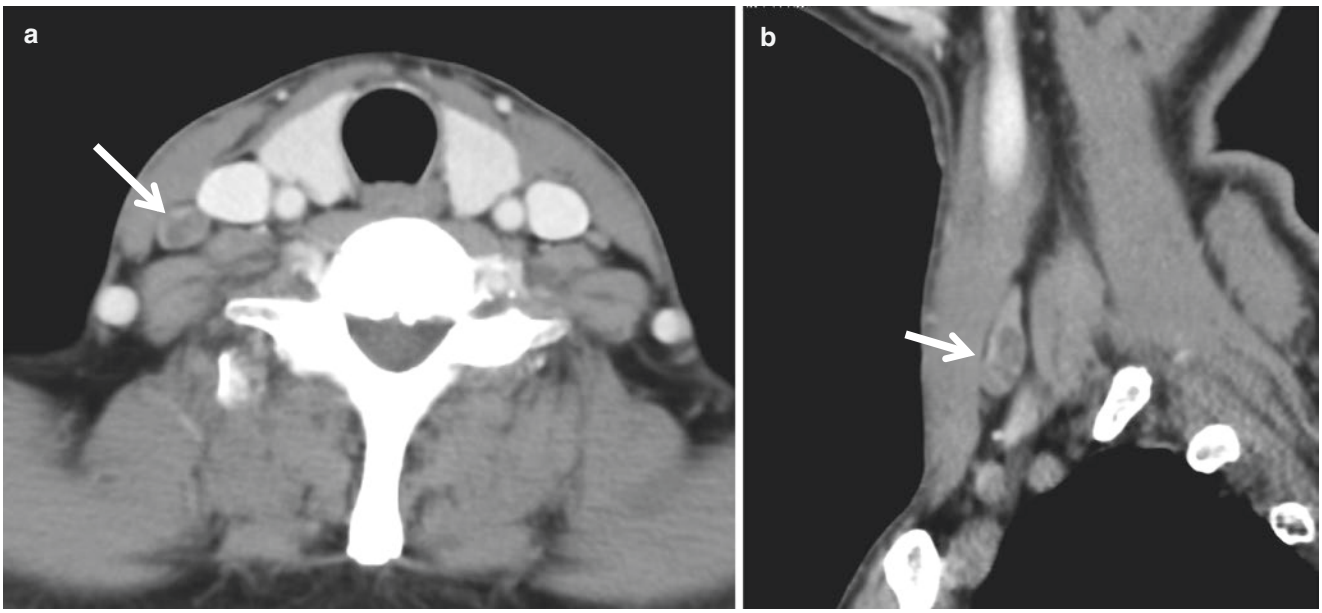

Fig. 6.6 Metastatic right level IV node (**a**, **b**, *arrow*) is less than 10 mm in minimum diameter and, however, has focal inhomogeneity

6.6.2 Shape

Nodal shape criteria are based on the pathologic observation that the normal or hyperplastic node is kidney-bean-shaped, whereas metastatic nodes are rounded. It has been suggested that the ratio of the maximum longitudinal nodal length to the maximum axial nodal length (L/T) should be greater than 2 for normal hyperplastic nodes, whereas a value of less than 2 strongly suggests that the node contains metastatic carcinoma (Fig. 6.4) [3, 16, 17]. If a lymph node is borderline by size criteria, but is round, it is more likely to be metastasis.

Normal nodes have usually well-defined borders and a fatty hilum that may be seen on CT, MRI, and US (Fig. 6.3). Malignant nodes typically show loss of the normal fatty hilum or focal cortical expansion (Figs. 6.4 and 6.6) [21]. However, focal cortical expansion is often found in normal or hyperplastic level IB nodes (Fig. 6.5).

6.6.3 Grouping

Nodal grouping is defined as the presence of three or more confluent lymph nodes with borderline size. Such a grouping along the expected drainage region is highly suggestive of metastasis [3]. When present, the minimal axial size threshold for a metastatic lymph node can be decreased by 1–2 mm, increasing sensitivity, without significantly affecting specificity.

6.6.4 Focal Nodal Inhomogeneity or Central Necrosis

The most reliable imaging criterion for metastatic lymphadenopathy is central necrosis. This term "central necrosis" is a misnomer, and the term "focal nodal inhomogeneity" is more suitable, because the medulla of metastatic nodes contain not only necrosis but also tumor cells [20, 22]. When the tumor metastasizes to the lymph nodes, these internal architecture become heterogeneous. As the majority of tumor cells enter a lymph node via the afferent lymphatics, focal nodal inhomogeneity occurs from the subcapsular region and spreads to the center of the node. If focal nodal inhomogeneity is >3 mm in size, it can frequently be identified on CT and MRI. Focal nodal inhomogeneity shows relatively low attenuation on CT and may appear hypointense on enhanced T1WI and hyperintense on T2WI and STIR images (Figs. 6.4 and 6.6).

The differential diagnosis of focal nodal inhomogeneity is the normal fatty hilum of the node. This hilum can be characterized as fatty attenuation on CT, as high intensity on T1WI and T2WIs, and as hyperechoic area on US (Figs. 6.3 and 6.5). The other differential diagnosis is an intranodal abscess in patients with acute infection and suppurative lymphadenitis. These cases are frequently evident based on the clinical presentation.

6.6.4.1 Cystic Nodal Metastasis

It has been recognized that there is a marked predilection for cystic nodal metastases to be associated with SCC of the tonsils and tongue base, and the incidence of cystic metastases has been reported to be as high as 33–50% [23]. The association between human papilloma virus (HPV) and tonsil and tongue base cancer has been well documented. HPV-related cancer accounts for more than 70% of HNSCC in oropharynx, and most of these cancers have cystic nodal metastases. In the unknown primary HNSCC with cystic nodal metastasis, primary tumors are often found in tonsils and tongue base. The mechanism of cyst formation in cystic nodal metastases has not been fully described. Radiologically, cystic nodes are defined as round or ovoid masses with a thin (<2 mm) enhancing capsule, homogeneous fluid content, and no internal complex, irregular, or solid area (Fig. 6.7). The differential diagnosis includes branchial cleft cyst and nodal metastasis of thyroid cancer.

6.6.5 Extranodal Extension (ENE)

Although terms such as extracapsular extension, extracapsular spread, or extranodal involvement have been used to denote tumor extension outside the capsule of a metastatic

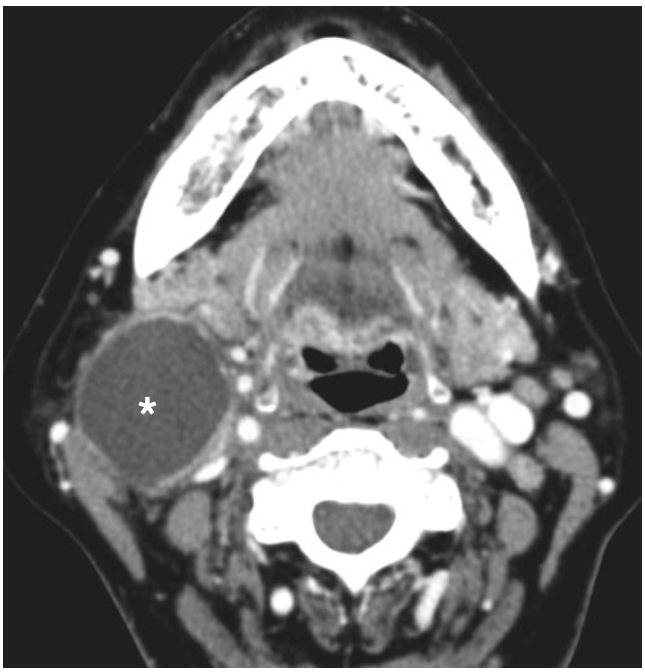

Fig. 6.7 Axial CECT image shows a cystic metastasis (*asterisk*) from HPV-related tongue base cancer. The lesion is similar to a second branchial cleft cyst

node, the American Joint Committee on Cancer (AJCC) and the Union for International Cancer Control (UICC) recommend extranodal extension (ENE) as a preferred wording.

The neck lymph node metastases decrease the overall survival by approximately half, and ENE worsens the prognosis by another 50% [24]. It was initially believed that extranodal extension occurred only in lymph nodes larger than 3 cm in greatest diameter. However, some studies have shown that ENE occurs in 23% on nodes less than 1 cm in greatest diameter, in 53% of nodes 2–3 cm in greatest diameter, and in 74% of nodes greater than 3 cm in greatest diameter. Overall, 60% of nodes with a greatest diameter of less than 3 cm have microscopic or gross extranodal extension [25, 26].

Several CT or MRI features suggest ENE, such as indistinct nodal margins and irregular nodal capsular enhancement; however, the strongest imaging feature supporting the clinical diagnosis for ENE is clear infiltration into the adjacent fat or muscle (Fig. 6.8). CT or MRI generally has low sensitivity (65–80%) but high specificity (86–93%) for the detection of ENE. On US, ENE is suggested by interrupted or undefined nodal contours. US appears to be less accurate in assessment of ENE than CT and MRI.

6.6.5.1 Carotid Arterial Invasion

The common or internal carotid artery is invaded in up to 5–10% of cervical lymph node metastasis of HNSCC [27]. Although it is important to recognize carotid invasion prior to treatment, it is often difficult. The size of metastatic lymph node is not a significant indicator of carotid invasion [28]. Deformity of the contour of carotid artery is a highly indicator of carotid arterial invasion. If the carotid artery is surrounded by a tumor above 270°, no surgical resection is generally attempted. However, it is often difficult to determine resectability by contact angle (Fig. 6.8). Surgical resection of tumor can be performed in cases without adventitial invasion of carotid artery. Because the carotid artery can be dissected from the tumor if the feeding vessels within the adventitia can be detected between the tumor and the carotid artery on enhanced CT, we consider that this finding is important. Even in cases with arterial invasion, resection and reconstruction of the carotid artery may result in better regional control. Therefore, it is important to select a treatment based on the comprehensive consideration including the patient's wishes and condition.

6.6.5.2 Prevertebral Fascia Invasion

The prevertebral fascia is tough and provides a barrier to tumor invasion. There have been previous reports of imaging findings on prevertebral fascia infiltration [29]. Compression and deformity of the fascia and signal changes of the prevertebral muscles on T2WI were considered as useful findings, but their specificities were low. The most reliable finding that indicates there is no invasion is that the fat of the retropharyngeal space is preserved.

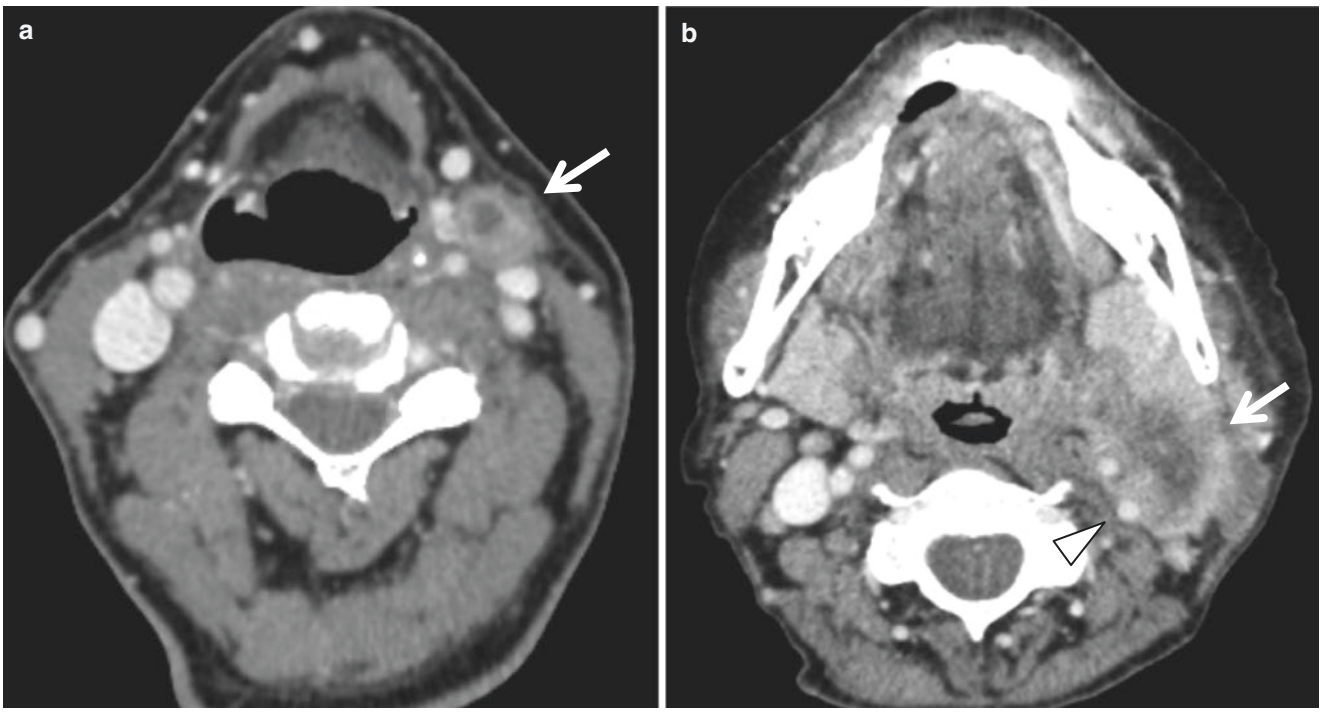

Fig. 6.8 Metastatic nodes reveal radiological ENE, such as enhancement of the nodal periphery, and irregular margins with infiltration to adjacent fat (**a**), or adjacent muscle planes and carotid artery (**b**). In b, the ICA (*arrowhead*) had 180° of contact with the metastatic node; however, adventitial invasion was confirmed at surgery

6.6.6 Vascular Patterns on US

Doppler US is the modality of choice for the assessment of a vascular pattern in neck cervical nodes. A hilar pattern is radiating vessels from the hilum into the node, and this pattern is highly specific for benign lymph nodes (Fig. 6.3) [30]. Non-hilar patterns include vascular displacement due to a focal intranodal lesion and a peripheral pattern due to neovascularization where vessels enter the node via the capsule away from the nodal hilum and are highly specific for metastatic involvement (Fig. 6.4).

6.7 Nodal Staging of HNSCC

TNM classification decided and revised by AJCC and UICC is widely accepted for cancer staging. This system has been classified based on the number, maximum size, and laterality of the affected nodes. After TNM classification seventh edition, HPV-related oropharyngeal cancer has been found to have several different characteristics, such as natural history, response to treatment, and prognosis. Radiation and chemoradiotherapy have been increased in HNSCC treatment. Based on these, the nodal staging of the TNM classification eighth edition instituted two major changes (Tables 6.3 and 6.4) [31, 32].

Table 6.3 Clinical N staging

Primary site	N stage	Definition
Any	NX	Regional nodes cannot be assessed
	N0	No regional nodal metastasis
All excluding p16+ oropharynx, and nasopharynx	N1	Single ipsilateral ≤3 cm ENE(−)
	N2a	Single ipsilateral >3 cm and ≤6 cm ENE(−)
	N2b	Multiple ipsilateral ≤6 cm ENE(−)
	N2c	Bilateral or contralateral ≤6 cm ENE(−)
	N3a	> 6 cm ENE(−)
	N3b	Any node(s) ENE(+)
p16+ oropharynx	N1	Unilateral ≤6 cm
	N2	Contralateral or bilateral ≤6 cm
	N3	>6 cm
Nasopharynx	N1	Unilateral cervical; unilateral or bilateral RPN; above the caudal border of cricoid cartilage ≤6 cm
	N2	Bilateral cervical; above the caudal border of cricoid cartilage ≤6 cm
	N3	Below the caudal border of cricoid cartilage >6 cm

The presence of skin involvement or soft tissue invasion with deep fixation/tethering to underlying muscle or adjacent structures or clinical signs of nerve involvement is classified as clinical ENE
ENE extranodal extension, *RPN* retropharyngeal node

Table 6.4 Pathological N staging

Primary site	N stage	Definition
Any	pNX	Regional lymph nodes cannot be assessed
	pN0	No regional lymph node metastasis
All excluding p16+ oropharynx, and nasopharynx	pN1	Single ipsilateral ≤3 cm ENE(−)
	pN2a	Single ipsilateral ≤3 cm ENE(+); Single ipsilateral >3 cm and ≤6 cm ENE(−)
	pN2b	Multiple ipsilateral ≤6 cm ENE(−)
	pN2c	Bilateral or contralateral ≤6 cm ENE(−)
	pN3a	>6 cm ENE(−)
	pN3b	Single ipsilateral >3 cm ENE(+); Multiple ENE(+)
p16+ oropharynx	pN1	1–4 lymph node(s)
	pN2	5 or more lymph nodes
Nasopharynx		Clinical N staging

ENE detected on histopathologic examination is designated as ENE_{mi} (microscopic ENE ≤2 mm) or EME_{ma} (major ENE >2 mm). Both $ENE_{mi\ and}$ EME_{ma} qualify as ENE(+) for definition of pN
ENE extranodal extension

The first change is that different clinical and pathological N classifications are proposed. Clinical N (cN) classification is required for all patients, and pathological N (pN) classification is only for patient undergoing surgery. Once involved node is identified on histopathological examination for patients undergoing surgery, pN is designated based on measurement of the largest dimension of the metastatic deposit and not of the entire lymph node. Pathological examination is necessary to record the location or level, the number of metastatic lymph nodes, and the presence and extent of ENE. An excisional biopsy of lymph node does not qualify for full evaluation of the pN category and should be assigned cN.

The second change is the use of extranodal extension (ENE). ENE has been known to be an important prognostic factor of nodal metastases in HNSCC, except for HPV-related tumors [33]. The eighth edition introduces ENE in the N category for both clinical and pathologic staging of HNSCC not related to HPV or EBV. Early ENE can only be identified on pathologic examination and cannot be reliably detected on clinical examination or with currently available imaging modality [34]. Therefore, The AJCC/UICC committee has set a high limitation for incorporating ENE into clinical staging. Clinical ENE requires overt clinical signs of gross (macroscopic) ENE supported by imaging findings (Fig. 6.8b). Obvious clinical signs of gross ENE include invasion of skin,

infiltration of musculature, dense tethering or fixation to adjacent structures, or cranial nerve, brachial plexus, sympathetic trunk, or phrenic nerve invasion with dysfunction. The presence of clinical ENE migrates them all uniformly to the new subcategory of cN3b (Table 6.3). Pathological ENE also will be clearly defined as extension of metastatic tumor beyond the confines of the lymph node, through the lymph node capsule into the surrounding connective tissue, regardless of the presence of stromal reaction. ENE detected on histopathologic examination is subcategorized as ENE_{mi} (microscopic ENE ≤2 mm from the nodal capsule) or ENE_{ma} (major or macroscopic ENE >2 mm beyond the nodal capsule, or a soft tissue deposit that has completely destroyed nodal architecture). Both ENE_{mi} and ENE_{ma} qualify as ENE-positive for the definition of pN. The presence of ENE in a single ipsilateral lymph node less than 3 cm in maximum dimension migrates that category to pN2a (Table 6.4).

6.7.1 Unknown Primary Tumor

The head and neck region is unique because several different staging classifications are based on anatomic site. The classification of unknown primary site has been improved by understanding the tumorigenesis of head and neck cancer and improvement of histologic methods to identify EBV-related and HPV-related tumors. Patients with EBV-related lymphadenopathy are staged according to nasopharyngeal cancer. Patients with HPV-related lymphadenopathy are staged according to HPV-related oropharyngeal cancer. All other patients with EBV-unrelated and HPV-unrelated lymphadenopathy are staged according to the N category of unknown primary tumor.

6.8 Treatment Assessment

6.8.1 Prediction of Treatment Response to (Chemo)Radiotherapy

Several findings that predict treatment effects and prognosis are obtained from functional imaging techniques performed before treatment or early in treatment. Regional control is more likely to occur in nodes with higher vascularity, as shown by higher K trans in dynamic MRI [35]. Tumor control is also seen in lymph nodes with lower pretreatment ADC and higher rise of ADC early in treatment (Fig. 6.9) [36, 37]. Using FDG-PET, primary tumors with lower SUV are more likely to show an overall response in the neck [38]. In addition, high FDG uptake before treatment in lymph node metastasis of HNSCC may be a risk factor for distant metastasis [39].

6.8.2 Assessment for Post (Chemo) Radiotherapy

Most HNSCC lymph node metastases respond completely to radiation or chemoradiotherapy (CRT). Previously, planned neck dissection was done after radiation or CRT. Fortunately, with the development of an effective chemotherapy regimen, neck dissection has only been performed in patients who have clinical evidence of residual disease after radiation or CRT. The selection of patients with posttreatment residual disease requiring early salvage surgery has become an important part of imaging.

The changes after radiation or CRT occur within 2 weeks of therapy and are initially an acute inflammatory response, which ultimately result in scar at 6 weeks to 1 year after treatment.

CT and MRI both have a high negative predictive value (94–97%) for residual nodal disease if the nodal metastases have essentially disappeared. However, lymph node metastases are often poorly regressive, leaving varying amounts of scar tissue. In CT-based studies, it has been reported that residual nodes of 15 mm or less without focal inhomogeneity or nodes with a reduction in size greater than 90% were associated with tumor control. However, even if the remaining lymph nodes exceed 15 mm, there may be no residual cancer. Therefore, focusing on the scar that occurred after treatment improves the accuracy of diagnosis. Scar tissue shows faint or absent enhancement and lower attenuation than surrounding muscles on contrast-enhanced CT. MRI is more useful than CT; scar tissue shows low signal intensity on T2WI, low signal intensity on DWI obtained with b of 0 s/mm^2 and b of 1000 s/mm^2 and low ADC value [40]. This low signal intensity is characteristic of benign scar tissue, indicating hyalinization, and should be differentiated from intermediate T2 signal intensity encountered in persistent lymph nodes at 6–8 weeks after treatment (Fig. 6.10).

FDG-PET/CT is increasing to assess lymph nodes after treatment and is performed at 10–12 weeks after treatment to prevent false positives or false negatives. FDG-PET/CT shows a high negative predictive value (96%) and is more accurate than CT and MRI, although the positive predictive value is low (49%) [41].

6.8.3 Posttreatment Surveillance

Because most recurrences occur within the first 2 years of treatment, close clinical and imaging surveillance is important for the detection of relapses (Fig. 6.11). Posttherapeutic baseline images are performed within

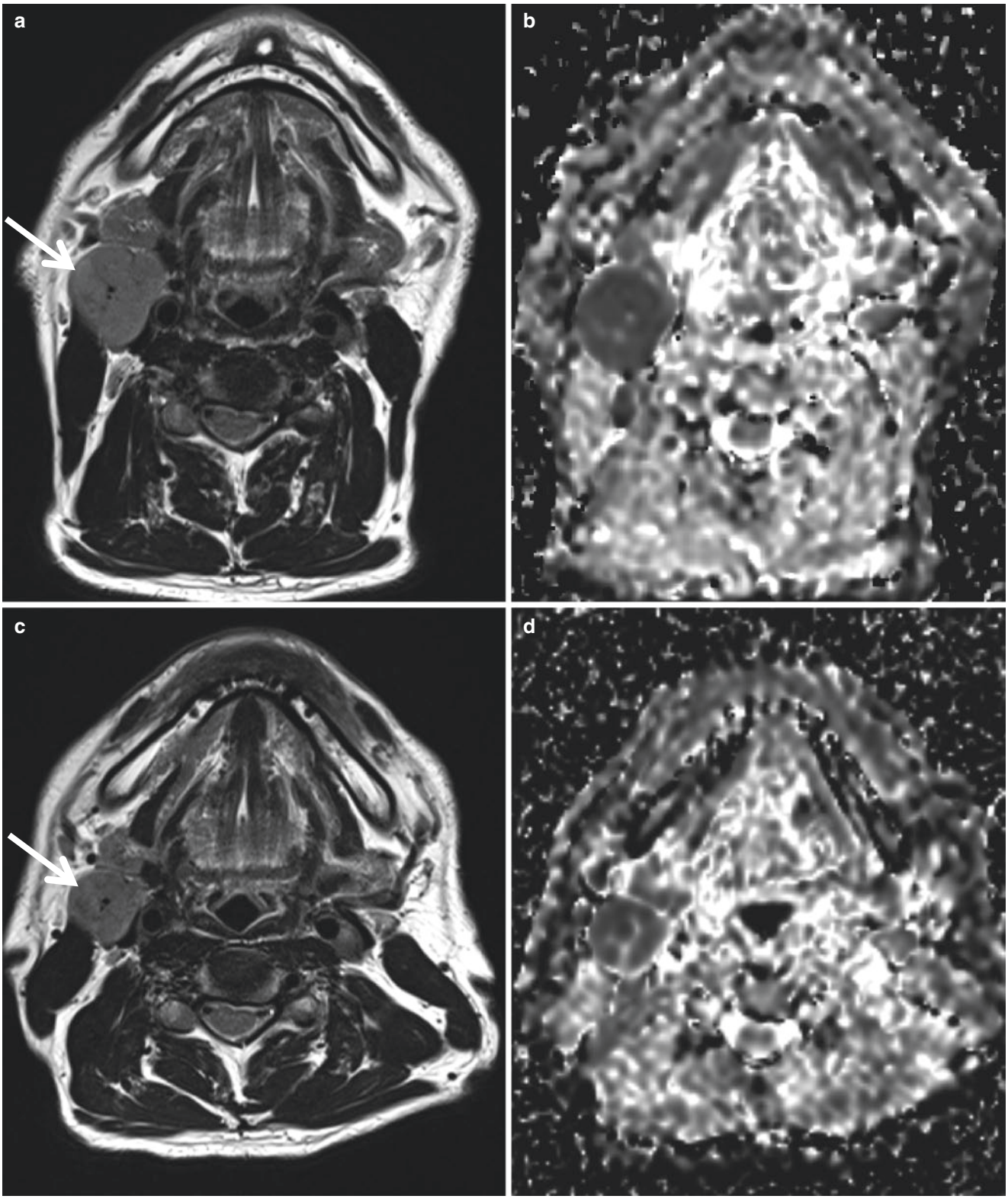

Fig. 6.9 Comparing the metastatic right level II lymph node before treatment (*top row*) and at 2 weeks with concomitant chemoradiotherapy (*bottom row*), the size of the node decreased and the ADC value increased 0.7×10^{-3} mm^2/s pretreatment to 1.1×10^{-3} mm^2/s at 2 weeks intra-treatment. This indicates increased diffusion, which favors a treatment response

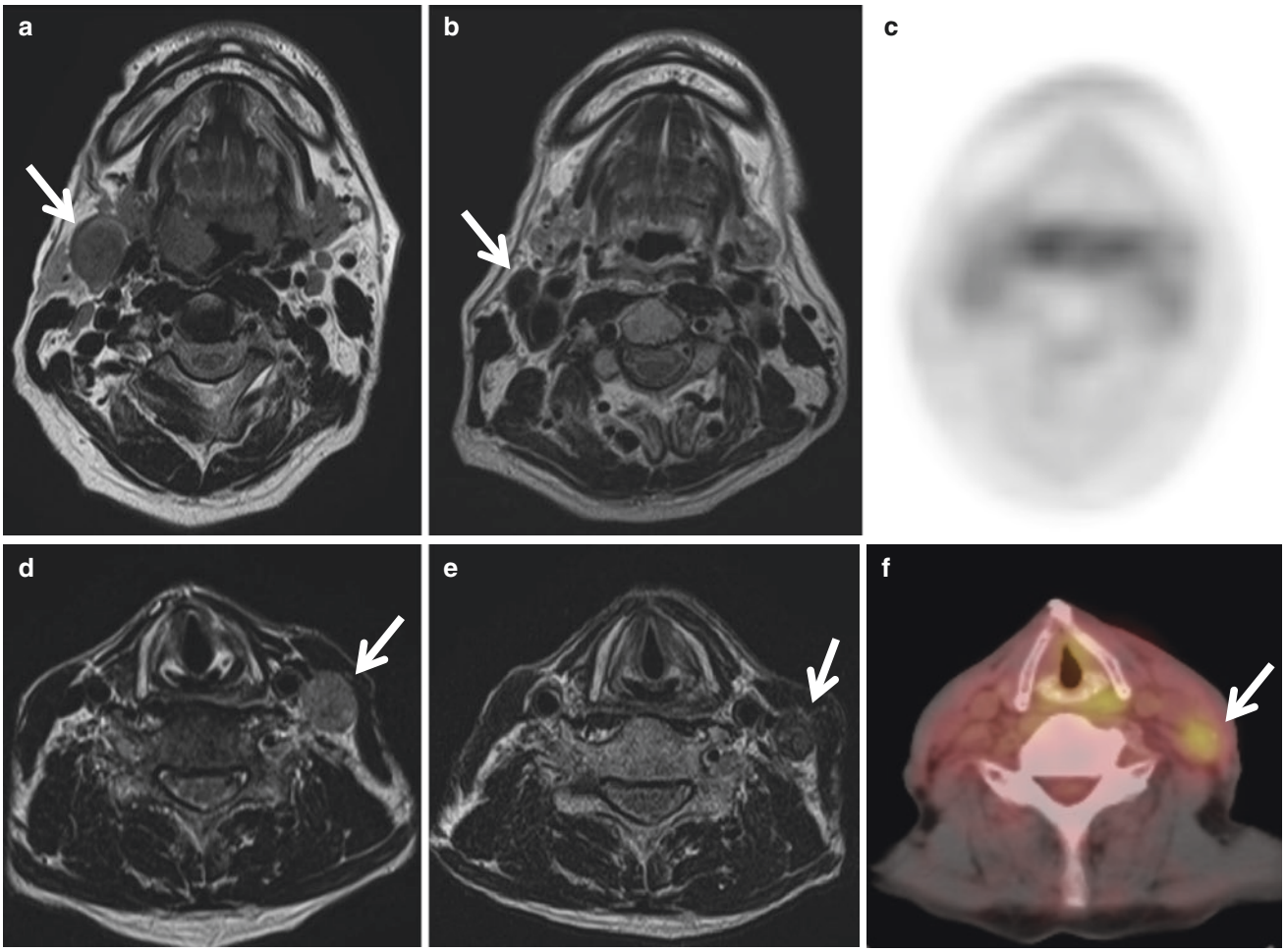

Fig. 6.10 Metastatic lymph node showing intermediate intensity before treatment has low intensity on T2WI and no FDG accumulation in CR case (*top row*). However, in non-CR case (*bottom row*), a metastatic node still shows intermediate intensity on T2WI and FDG accumulation after treatment

4–8 weeks after treatment, and the patients generally undergo imaging every 3–6 months for 2–3 years, being more frequent in the earlier posttreatment period.

The effects of surgery, radiation, and chemotherapy can drastically alter the normal anatomy [42, 43]. Altered tissue after treatment and recurrent nodes may show mimic findings. Lymph node metastasis may occur in unexpected areas, as lymphatics also changes after treatment. Some relapses may occur from occult metastasis. Therefore, it is important to compare the baseline image and the follow-up image to obtain valuable information in the interpretation.

Although the imaging modality used to monitor HNSCC patients is variable, CT or MRI is generally performed. CT has a high sensitivity and moderate specificity for differentiating recurrence from posttreatment changes. If it is difficult to distinguish recurrence from posttreatment changes on CT, DWI may be useful as recurrent nodal diseases show restricted diffusion with low ADCs. US-FNAC also plays a role in posttreatment surveillance and early detection of potential lymph node metastases, increasing the possibility of performing salvage surgery with US follow-up. Now, there are also institutions that perform FDG-PET routinely as a posttreatment baseline or for patients with suspected recurrent disease on conventional imaging. Inflammatory or infectious conditions can lead to false-positive PET finding; no FDG-PET/CT should be performed without knowledge of clinical findings.

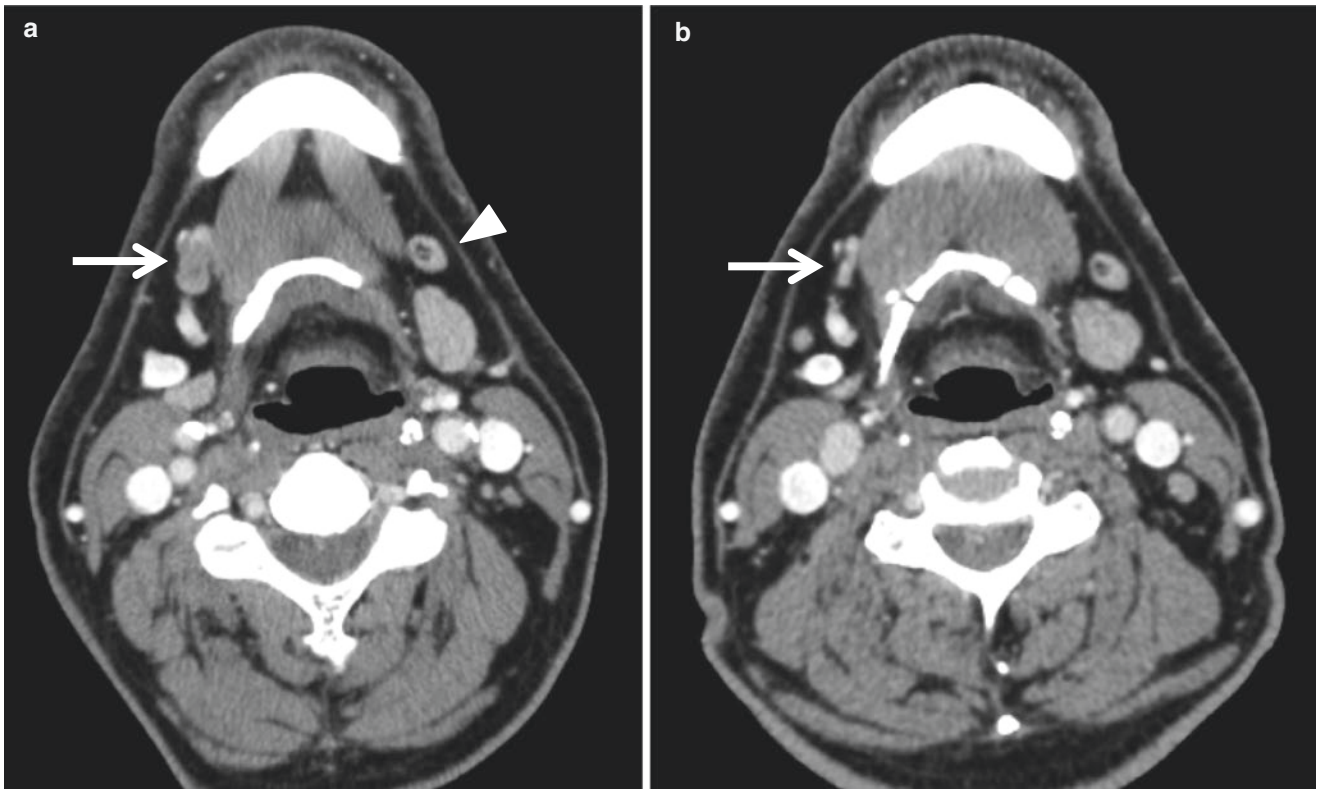

Fig. 6.11 Axial follow-up CECT 6 months after surgery of tongue cancer (**a**) shows a metastatic lymph node (*arrow*) with focal inhomogeneity in right level IB. Before treatment (**b**), this node (*arrow*) is in normal size and attenuation. Left level IB lymph node (**a**, *arrowhead)* shows no change in morphology before and after treatment

References

1. Rouvière H. Lymphatic system of the head and neck. Ann Arbor, MI: Edwards Brothers; 1938. p. 5–28.
2. Som PM, Curtin HD, Mancuso AA. An imaging-based classification for the cervical nodes designed as an adjunct to recent clinically based nodal classifications. Arch Otolaryngol Head Neck Surg. 1999;125:388–96.
3. van den Brekel M, Stel H, Castelijns J, Nauta JJ, Van der Waal I, Valk J, et al. Cervical lymph node metastasis: assessment of radiologic criteria. Radiology. 1990;177:379–84.
4. Byers RM, Weber RS, Andrews T, McGill D, Kare R, Wolf P. Frequency and therapeutic implications of "skip metastases" in the neck from squamous carcinoma of the oral tongue. Head Neck. 1997;19:14–9.
5. Melkane AE, Mamelle G, Wycisk G, Temam S, Janot F, Casiraghi O, et al. Sentinel node biopsy in early oral squamous cell carcinomas: a 10-year experience. Laryngoscope. 2012;122:1782–8.
6. Wang Y, Ow TJ, Myers JN. Pathways for cervical metastasis in malignant neoplasms of the head and neck region. Clin Anat. 2012;25:54–71.
7. Sumi M, Ohki M, Nakamura T. Comparison of sonography and CT for differentiating benign from malignant cervical lymph nodes in patients with squamous cell carcinoma of the head and neck. Am J Roentgenol. 2001;176:1019–24.
8. Curtin HD, Ishwaran H, Mancuso AA, Dalley RW, Caudry DJ, McNeil BJ. Comparison of CT and MR imaging in staging of neck metastases. Radiology. 1998;207:123–30.
9. Thoeny HC, De Keyzer F, Kinf AD. Diffusion-weighted MR imaging in the head and neck. Radiology. 2012;263:19–32.
10. Vandecaveye V, Keyzer FD, Pooten VV, Dirix P, Verbeken E, Nuyts S, et al. Head and neck squamous cell carcinoma: value of diffusion-weighted MR imaging for nodal staging. Radiology. 2009;251:134–46.
11. Dirix P, Vandecaveye V, De Keyzer F, de Beeck KO, Pooten VV, Delaere P, et al. Diffusion-weighted MRI for nodal staging of head and neck squamous cell carcinoma: impact on radiotherapy planning. Int J Radiat Oncol Biol Phys. 2010;76:761–6.
12. Jeong HS, Baek CH, Son YI, Chung MK, Lee DK, Choi JY, et al. Use of integrated 18F-FDG PET/CT to improve the accuracy of initial cervical nodal evaluation in patients with head and neck squamous cell carcinoma. Head Neck. 2007;29:203–10.
13. Gordin A, Golz A, Keidar Z, Daltzchman M, Shalom RB, Israel O. The role of FDG-PET/CT imaging in head and neck malignant conditions: impact on diagnostic accuracy and patient care. Otolaryngol Head Neck Surg. 2007;137:130–7.
14. Adams S, Baum RP, Stuckensen T. Prospective comparison of 18F-FDG PET with conventional imaging modalities (CT, MRI, US) in lymph node staging of head and neck cancer. Eur J Nucl Med. 1998;25:1255–60.
15. Stoeckli SJ, Steiner H, Pfaltz M, Schmid S. Is there a role for positron emission tomography with 18F-fluorodeoxyglucose in the initial staging of nodal negative oral and oropharyngeal squamous cell carcinoma. Head Neck. 2002;24:345–9.
16. Snow GB, Annyas AA, Van Slooten EA, Bartelink H, Hart AA. Prognostic factors of neck node metastasis. Clin Otolaryngol. 1982;7:185–92.

17. Som PM. Detection of metastasis in cervical lymph nodes: CT and MR criteria and differential diagnosis. Am J Roentgenol. 1992;158:961–9.
18. Mancuso A, Harnsberger H, Muraki Am Stevens M. Computed tomography of cervical and retropharyngeal lymph nodes: normal anatomy, variants of normal, and application in staging head and neck cancer. Part II. Radiology. 1983;148:715–23.
19. Mizowaki T, Nishimura Y, Shimada Y, Nakano Y, Imamura M, Konishi J, et al. Optimal size criteria of malignant lymph nodes in the treament planning of radiotherapy for esophageal cancer; evaluation by computed tomography and magnetic resonance imaging. Int J Radiat Oncol Biol Oncol Biol Phys. 1996;36:1091–8.
20. van den Brekel MW, Castelijins JA, Snow GB. The size of lymph nodes in the neck on sonograms as a radiologic criterion for metastasis: how reliable is it? Am J Neuroradiol. 1998;19:695–700.
21. Forghani R, Curtin HD. Imaging evaluation of cervical lymph nodes. In: Yu E, Shankar L, editors. Introductory head and neck imaging. New Delhi: Jaypee Brochers Medical Publishers; 2014. p. 421–504.
22. Rubaltelli L, Proto E, Salmaso R, Bortoletto P, Candiani F, Cagol P. Sonography of abnormal lymph nodes in vitro; correlation of sonographic and histologic findings. Am J Roentgenol. 1990;155:1241–4.
23. Som PM, Brandwein-Gensler MS. Lymph nodes of the neck. In: Som PM, Curtin HD, editors. Head and neck imaging. St. Louis: Mosby; 2011. p. 2287–383.
24. Regauer S, Mannweiler S, Anderhuber W, Gotschuli A, Berghold A, Schachenreiter J, et al. Cystic lymph node metastases of squamous cell carcinoma of Waldeyer's ring origin. Br J Cancer. 1999;79:1437–42.
25. Bataskis JG. Squamoud cell carcinoma of the oral cavity and the oropharynx. In: Tumor of the head and neck: clinical and pathological considerations. 2nd ed. Baltimore: Williams & Wilkins; 1979. p. 144–76.
26. Chong V. Cervical lymphadenoathy: what radiologists need to know. Cancer Imaging. 2004;4:116–20.
27. Nemeth Z, Domotor G, Talos M. Resection and head and neck cancer. Int J Oral Maxillofac Surg. 2003;32:645–50.
28. Pons Y, Ukkola-Pons E, Clement P, Gauthler J, Conessa C. Relevance of 5 different imaging signs in the evaluation of carotid artery invasion by cervical lymphadenopathy in head and neck squamous cell carcinoma. Oral Surg Oral Med Oral Pathol Oral Radiol Endod. 2010;109:775–8.
29. Loevner LA, Ott IL, Yousem SM, Montone KT, Thaler ER, Chalian AA, et al. Neoplastic fixation to the prevertebral compartment by squamous cell carcinoma of the head and neck. Am J Roentogenol. 1998;170:1389–94.
30. Ahuja A, Ying M. Sonographic evaluation of cervical lymphadenopathy: is power Doppler sonography routinely indicated? Ultrasound Med Biol. 2003;29:353–9.
31. Amin MB, Edge SB, Greene FL, Byrd DR, Brookland RK, Washington MK, et al. American Joint Committee on Cancer manual for staging of cancer. 8th ed. New York: Springer; 2017.
32. Brierley JD, Gospodarowicz MK, Wittekind C. Union for International Cancer Control TNM classification of malignant tumours. 8th ed. New York: Wiley; 2017.
33. Liu JT, Kann BH, De B, Buckstein M, Bakst RL, Genden EM, et al. Prognostic value of radiographic extracapsular extension in locally advanced head and neck squamous cell cancers. Oral Oncol. 2016;52:52–7.
34. Prabhu RS, Magliocca KR, Hanasoge S, Aiken AH, Hudgins PA, Hall WA, et al. Accuracy of computed tomography for predicting pathologic nodal extracapsular extension in patients with head-and-neck cancer undergoing initial surgical resection. Int J Radiat Oncol Biol Phys. 2014;88:122–9.
35. Kim S, Loevner LA, Quon H, Kilger A, Sherman E, Weinstein G, et al. Prediction of response to chemoradiation therapy in squamous cell carcinomas of the head and neck using dynamic contrast-enhanced MR imaging. Am J Neuroradiol. 2010;31:262–8.
36. Vandecaveye V, Dirix P, De Keyzer F, de Beeck KO, Poorten VV, Roebben I, et al. Predictive value of diffusion-weighted magnetic resonance imaging during chemoradiotherapy for head and neck squamous cell carcinoma. Eur Radiol. 2010;20:1703–14.
37. Noji DP, Martens RM, Marcus JT, de Bree R, Leemans R, Castelijns JA, et al. Intravoxel incoherent motion magnetic resonance imaging in head and neck cancer: a systematic review of the diagnostic and prognostic value. Oral Oncol. 2017;68:81–91.
38. Schwartz DL, Rajendran J, Yueh B, Coltrera M, Anzai Y, Krohn K, et al. Staging of head and neck squamous cell cancer with extended-field FDG-PET. Arch Otolaryngol Head Neck Surg. 2003;129:1173–8.
39. Kubicek GJ, Champ C, Fogh S, Wang F, Reddy E, Intenzo C, et al. FDG-PET staging and importance of lymph node SUV in head and neck cancer. Head Neck Oncol. 2010;2:19–25.
40. King AD, Keung CK, Yu KH, Mo FKF, Bhatia KS, Yeung DKW, et al. T2-weighted MR imaging early after chemoradiotherapy to evaluate treatment response in head and neck squamous cell carcinoma. Am J Neuroradiol. 2013;34:1237–41.
41. Isles MG, McConkey C, Mehanna HM. A systematic review and meta-analysis of the role of positron emission tomography in the follow up of head and neck squamous cell carcinoma following radiotherapy or chemoradiotherapy. Clin Otolaryngol. 2008;33:210–22.
42. Hadgins PA. Flap reconstruction in the head and neck: expected appearance, complications, and recurrent disease. Eur J Radiol. 2002;44:130–8.
43. Offiah C, Hall E. Post-treatment imaging appearances in head and neck cancer patients. Clin Radiol. 2011;66:13–24.